

# Ground State Phase Diagram of Generic $XY$ Pyrochlore Magnets with Quantum Fluctuations

Anson W. C. Wong,<sup>1,2</sup> Zhihao Hao,<sup>2</sup> and Michel J. P. Gingras<sup>2,3,4</sup>

<sup>1</sup>*Department of Physics and Astronomy, University of British Columbia, Vancouver, BC, V6T 1Z1, Canada*

<sup>2</sup>*Department of Physics and Astronomy, University of Waterloo, Waterloo, ON, N2L 3G1, Canada*

<sup>3</sup>*Perimeter Institute for Theoretical Physics, 31 Caroline North, Waterloo, ON, N2L 2Y5, Canada*

<sup>4</sup>*Canadian Institute for Advanced Research, 180 Dundas Street West, Suite 1400, Toronto, ON, M5G 1Z8, Canada*

(Dated: November 7, 2018)

Motivated by recent experimental and theoretical progress on the  $\text{Er}_2\text{Ti}_2\text{O}_7$  pyrochlore  $XY$  antiferromagnet, we study the problem of quantum order-by-disorder in pyrochlore  $XY$  systems. We consider the most general nearest-neighbor pseudo spin-1/2 Hamiltonian for such a system characterized by anisotropic spin-spin couplings  $J_e \equiv \{J_\pm, J_{\pm\pm}, J_{z\pm}, J_{zz}\}$  and construct zero-temperature phase diagrams. Combining symmetry arguments and spin-wave calculations, we show that the ground state phase boundaries between the two candidate ground states of the  $\Gamma_5$  irreducible representation, the  $\psi_2$  and  $\psi_3$  (basis) states, are rather accurately determined by a cubic equation in  $(J_\pm J_{\pm\pm})/J_{z\pm}^2$ . Depending on the value of  $J_{zz}$ , there can be one or three phase boundaries that separate alternating regions of  $\psi_2$  and  $\psi_3$  states. In particular, we find for sufficiently small  $J_{zz}/J_\pm$  a narrow  $\psi_2$  sliver sandwiched between two  $\psi_3$  regions in the  $J_{\pm\pm}/J_\pm$  vs  $J_{z\pm}/J_\pm$  phase diagram. From our results, one would be able to predict which state ( $\psi_2$  or  $\psi_3$ ) may be realized in a real material given its set of  $J_e$  couplings. Our results further illustrate the very large potential sensitivity of the ground state of  $XY$  pyrochlore systems to minute changes in their spin Hamiltonian. Finally, using the experimentally determined  $J_e \equiv \{J_\pm, J_{\pm\pm}, J_{z\pm}, J_{zz}\}$  and  $g$ -tensor values for  $\text{Er}_2\text{Ti}_2\text{O}_7$ , we show that the heretofore neglected long-range  $1/r^3$  magnetostatic dipole-dipole interactions do not change the conclusion that  $\text{Er}_2\text{Ti}_2\text{O}_7$  has a  $\psi_2$  ground state induced via a quantum order-by-disorder mechanism. As a new avenue of research in  $XY$  pyrochlore materials distinct from the rare-earth pyrochlore oxides, we propose that the  $\text{Cd}_2\text{Dy}_2\text{Se}_4$  chalcogenide spinel, in which the  $\text{Dy}^{3+}$  ions form a pyrochlore lattice and may be  $XY$ -like, could prove interesting to investigate.

## I. INTRODUCTION

Simplified Hamiltonian ( $\mathcal{H}$ ) models of magnetic systems with competing or geometrically frustrated interactions often feature a large number of accidentally degenerate classical ground states. Such a degeneracy can typically be lifted energetically by additional perturbations to  $\mathcal{H}$ , such as further neighbor interactions, magnetic anisotropy as well as spin-lattice coupling<sup>1</sup>. A more exotic mechanism is one in which thermal or quantum fluctuations induce long-range order within the degenerate manifold. This is the thermal or quantum order-by-disorder (ObD) mechanism<sup>2-5</sup>.

While thermal<sup>2</sup> and quantum<sup>3</sup> ObD has been proposed to be at play in a number of condensed matter systems, the number of compelling experimental demonstrations of ObD among real materials, as opposed to theoretical models, has remained quite limited. In this context, the  $\text{Er}_2\text{Ti}_2\text{O}_7$  insulating magnetic pyrochlore oxide<sup>6</sup> stands as a promising textbook example where ObD is at the origin of the experimentally observed long-range order.

In  $\text{Er}_2\text{Ti}_2\text{O}_7$ , the magnetic  $\text{Er}^{3+}$  ions form a three-dimensional network of corner-sharing tetrahedra, the so-called “pyrochlore” lattice<sup>6</sup>. A free  $\text{Er}^{3+}$  ion has angular momentum  $J = 15/2$ . The  $^4I_{15/2}$  multiplet splits in the local crystal-field environment, yielding a Kramers doublet as lowest energy levels<sup>7</sup>. The resulting pseudo spin-1/2 moment describing this magnetic doublet lies preferentially in an  $xy$  plane (see Fig. 1) perpendicular to the three-fold symmetry  $\hat{z}$  axis at the ion site, which is one of the cubic  $[111]$  directions.  $\text{Er}_2\text{Ti}_2\text{O}_7$  undergoes a second order transition to long-range order at a critical temperature  $T_c \approx 1.2 \text{ K}$ <sup>7-11</sup>. Defining  $\phi_r$  as the azimuthal angle of the magnetic moment in the  $xy$  plane

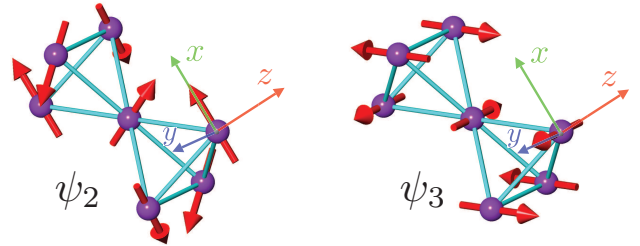


FIG. 1: Spin configurations of  $\psi_2$  (left) and  $\psi_3$  (right) states. See main text for description of the spin orientation for each state.

expressed in specific sublattice coordinates<sup>12</sup> for site  $r$ , neutron scattering studies<sup>7,13</sup> determined that  $\text{Er}_2\text{Ti}_2\text{O}_7$  orders in a state with  $\phi_r = \phi = n\pi/3$  ( $n = 0, 1, 2, \dots$ ), the so-called  $\psi_2$  state (see Fig. 1, left), in contrast to the  $\psi_3$  state with  $\phi = \pi/2 + n\pi/3$  (see Fig. 1, right). Both  $\psi_2$  and  $\psi_3$  are basis states of the  $\Gamma_5$  irreducible representation (irrep.)<sup>13</sup>, referred to as the  $\Gamma_5$  manifold hereafter. While it had been recognized for some time that quantum ObD might be at work in  $\text{Er}_2\text{Ti}_2\text{O}_7$ <sup>7,14</sup>, the details via which ObD does actually operate and select the non-coplanar  $\psi_2$  state had remained a central unsolved problem until recently<sup>15-18</sup>.

Much progress has been achieved over the past year<sup>17,18</sup> in reaching a resolution of this quandary. Building on previous works<sup>15,16</sup>, Refs. [17,18] showed that quantum ObD can select a  $\psi_2$  state in effective spin-1/2 models with anisotropic exchange interactions and relevant to  $\text{Er}_2\text{Ti}_2\text{O}_7$ . In particular, Savary *et al.*<sup>18</sup> obtained a microscopic pseudo spin-1/2 model of  $\text{Er}_2\text{Ti}_2\text{O}_7$  by fitting the spin-wave spectrum of a field-polarized paramagnetic state measured using inelastic

neutron scattering. These authors pointed out that no mechanism exists at the mean-field level via which arbitrary range anisotropic interactions can lift the degeneracy between  $\psi_2$  and  $\psi_3$ <sup>19</sup>. On the basis of their  $\text{Er}_2\text{Ti}_2\text{O}_7$ -parametrized model, Ref. [18] showed that quantum fluctuations select a  $\psi_2$  ground state as observed in  $\text{Er}_2\text{Ti}_2\text{O}_7$ <sup>7,13</sup>. We show below that including long-range dipolar interactions does not change this conclusion.

These recent developments have motivated us to study the following question: *Given a pyrochlore XY magnet where the  $\Gamma_5$  manifold has the lowest classical energy, which state,  $\psi_2$  or  $\psi_3$ , is selected by quantum fluctuations at temperatures close to zero?* In addition to its broad relevance to the field of frustrated magnetism, this question is of importance to help understand the ground state displayed by real magnetic pyrochlore compounds<sup>6</sup>.

To address this question, we investigate the most general symmetry-allowed Hamiltonian of Eq. (1) below<sup>12,20</sup> with nearest-neighbor bilinear spin interactions on the pyrochlore lattice. For the interaction parameters where the ground state belongs to the  $\Gamma_5$  manifold, we determine the phase boundaries of the  $\psi_2$  and  $\psi_3$  states by comparing the contribution of the quantum zero-point energy from spin-waves. Combining the spin-wave results with symmetry arguments, we show that, depending on the value of the anisotropic couplings, either  $\psi_2$  or  $\psi_3$  can be selected by quantum fluctuations. This is consistent with previous Monte-Carlo studies<sup>16,17,21</sup> for specific sets of interaction parameters where the ground state was found to be either  $\psi_2$  or  $\psi_3$ .

The rest of the paper is organized as follows. In Sec. II, we present the model and describe the main features of its phase diagram based on symmetry arguments. We use spin wave calculations to map out the phase diagram quantitatively in Sec. III. We find that  $\text{Er}_2\text{Ti}_2\text{O}_7$  sits deep in the  $\psi_2$  part of the phase diagram. In Sec. IV, we show that long-range dipolar interaction does not change the  $\psi_2$  ground state selection in  $\text{Er}_2\text{Ti}_2\text{O}_7$ . Finally, Sec. V concludes our paper and discusses future directions, proposing in particular that  $\text{CdDy}_2\text{Se}_4$  could be an interesting material to explore the physics of XY pyrochlore magnets outside the realm of the  $R_2\text{M}_2\text{O}_7$  pyrochlore oxides<sup>6</sup>.

## II. MODEL AND SYMMETRY CONSIDERATIONS

We consider the effective  $S = 1/2$  spin Hamiltonian  $\mathcal{H} = \mathcal{H}_0 + \mathcal{H}_1$  on the pyrochlore lattice with anisotropic nearest-neighbor exchange couplings  $J_e \equiv \{J_\pm, J_{\pm\pm}, J_{z\pm}, J_{zz}\}$ <sup>12</sup>:  $\mathcal{H} = \mathcal{H}_0 + \mathcal{H}_1$ <sup>12</sup>:

$$\mathcal{H}_0 = -J_\pm \sum_{\langle ij \rangle} (S_i^+ S_j^- + h.c.) + J_{zz} \sum_{\langle ij \rangle} S_i^z S_j^z \quad (1a)$$

$$\mathcal{H}_1 = \sum_{\langle ij \rangle} J_{\pm\pm} (\gamma_{ij} S_i^+ S_j^+ + \gamma_{ij}^* S_i^- S_j^-) + J_{z\pm} (S_i^z (\zeta_{ij} S_j^+ + \zeta_{ij}^* S_j^-) + i \leftrightarrow j), \quad (1b)$$

where  $\gamma_{ij} = -\zeta_{ij}^*$  are bond-dependent phases<sup>12,20</sup> (Appendix A). All spin components are written in terms of local coordi-

nates (see Fig. 1). If  $\mathcal{H}_1$  is absent and  $J_{zz} = 0$ ,  $\mathcal{H}$  in Eq. (1) reduces to a ferromagnetic XY model (in terms of spin components in the local coordinates) for which the XY ( $U(1)$ ) symmetry is exact. In other words,  $\mathcal{H}_0$  is invariant under a simultaneous rotation about all local  $z$  ([111]) axes. As a result, the  $\psi_2$  and  $\psi_3$  states have the same classical ground state energy. We observe that  $J_\pm$  is the primary interaction that favors  $\Gamma_5$  as lowest energy manifold and note, incidentally, that  $J_\pm$  is the largest coupling in  $\text{Er}_2\text{Ti}_2\text{O}_7$ <sup>18</sup>. In the remainder of the paper we set  $J_\pm = 1$ , with all energies henceforth measured in units of  $J_\pm$ , denoting the scaled interactions by the corresponding lower-case letters,  $j_{zz} \equiv J_{zz}/J_\pm$  for example.

A finite  $j_{zz}$  does not break the  $U(1)$  symmetry and the consequential Ising couplings  $J_{zz} S_i^z S_j^z$  are thus part of  $\mathcal{H}_0$  in Eq. (1). The character of the ground state changes, however, from XY-like to Ising-like if the magnitude of  $j_{zz}$  exceeds certain critical values: Two-in/two-out spin-ice states<sup>22</sup> are the lowest energy states for  $j_{zz} > 6$  while the ground state becomes the all-in-all-out<sup>22</sup> state if  $j_{zz} < -2$ .

The lattice is not invariant under an arbitrary rotation about the local  $z$  ([111] cubic) axes. This allows for a finite  $\mathcal{H}_1$  that breaks the  $U(1)$  symmetry *explicitly*<sup>18</sup>. In addition to Ising-like states, the  $\Gamma_5$  manifold is adjacent to several other phases in the parameter space spanned by  $j_{z\pm}$ ,  $j_{\pm\pm}$  and  $j_{zz}$ . For  $j_{\pm\pm} > 2$ , the Palmer-Chalker (PC) state<sup>23</sup> (i.e. the  $\psi_4$  state of the  $\Gamma_7$  irrep.<sup>13</sup>) is the ground state. Simple energy minimization determines the phase boundary between the  $\Gamma_5$  manifold and a state with ferromagnetic moments canted from the [100] cubic direction, or “splayed ferromagnetic” (SF) state<sup>20,24</sup>.

$$j_{\pm\pm}^{(\Gamma_5)} = \frac{4j_{z\pm}^2}{6 - j_{zz}} - 2. \quad (2)$$

The  $\Gamma_5$  with degenerate  $\psi_2$  and  $\psi_3$  states is realized in a range of  $j_{\pm\pm}$  that satisfies  $j_{\pm\pm}^{(\Gamma_5)} < j_{\pm\pm} < 2$ .

Within  $\Gamma_5$ , the energy of  $\psi_2$  and  $\psi_3$  remains the same at the classical level for arbitrary  $(J_\pm, J_{\pm\pm}, J_{z\pm}, J_{zz})$ <sup>18</sup>. This *accidental* degeneracy is expected to be generically lifted by quantum fluctuations. To lowest order, the energy contribution from quantum fluctuations is the sum of the zero-point energy of spin-wave modes, denoted as  $E_0(\psi_i)$  with  $i = 2, 3$ . Before describing the results of our spin-wave calculations, it is instructive to investigate the expected analytical properties of  $\delta E(j_{\pm\pm}, j_{z\pm}) \equiv E_0(\psi_2) - E_0(\psi_3)$  on the basis of a symmetry analysis.

Consider first  $\delta E(j_{\pm\pm}, 0)$ ; a rotation about the local  $z$  axes by  $\pi/2$  transforms  $\phi \rightarrow \phi + \pi/2$ . Consequentially,  $j_{\pm\pm}$  transforms as  $j_{\pm\pm} \rightarrow j_{\pm\pm} \exp(i\pi) = -j_{\pm\pm}$  while the spin configurations of the  $\psi_2$  and  $\psi_3$  states are interchanged:

$$\begin{aligned} \delta E(j_{\pm\pm}, 0) &\rightarrow \delta E(-j_{\pm\pm}, 0) = E_0(\psi_3) - E_0(\psi_2) \\ &= -\delta E(j_{\pm\pm}, 0). \end{aligned} \quad (3)$$

We conclude that  $\delta E(j_{\pm\pm}, 0)$  is an odd function of  $j_{\pm\pm}$ . Similarly, a rotation about the local  $z$  axes by  $\pi$  changes  $\phi \rightarrow \phi + \pi$ . Under this transformation,  $j_{z\pm} \rightarrow j_{z\pm} \exp(i\pi) = -j_{z\pm}$  and  $j_{\pm\pm} \rightarrow j_{\pm\pm}$ , with the  $\psi_2$  and  $\psi_3$  states preserved under this rotation, and  $\delta E(j_{\pm\pm}, j_{z\pm})$  is thus an even function of  $j_{z\pm}$ .

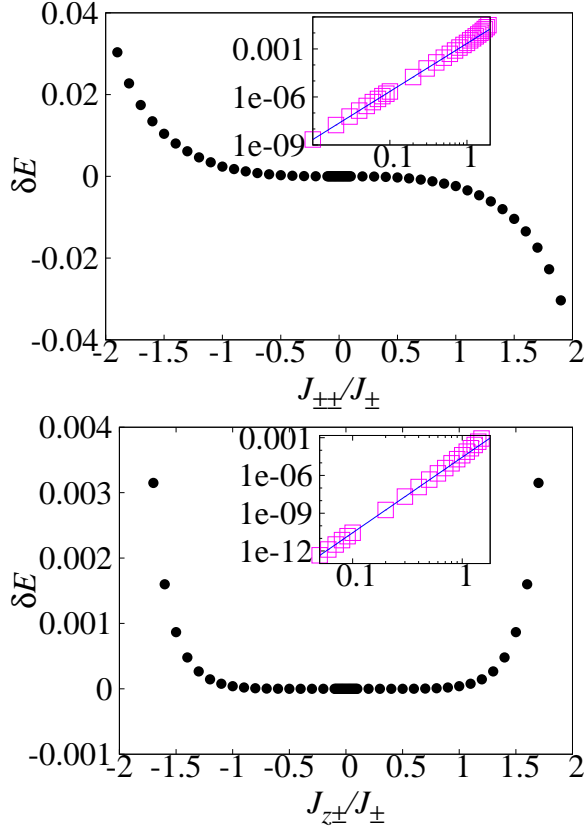


FIG. 2:  $\delta E(j_{\pm\pm}, 0)$  (top) is an odd function of  $j_{\pm\pm}$  and  $\delta E(0, j_{z\pm})$  (bottom) is an even function of  $j_{z\pm}$ . The insets show, in the form of log-log plots, the fit (solid blue line) of  $|\delta E(j_{\pm\pm}, 0)|$  to  $j_{\pm\pm}^3$  and  $\delta E(0, j_{z\pm})$  to  $j_{z\pm}^3$  for  $j_{\pm\pm} > 0$  and  $j_{z\pm} > 0$ , respectively. The fits (blue solid lines) were performed over the range  $[0.01, 0.1]$  for both  $j_{\pm\pm}$  and  $j_{z\pm}$ . The deviation of the data (symbols) from the fit reflects the slight departure of  $\delta E(\phi)$  from the strict  $\cos(6\phi)$  form and thus the cubic polynomial in  $x$  in Eq. (4).

These symmetry properties constrain the overall topology of the phase diagram for  $-2 < j_{zz} < 6$ .

Symmetry considerations also help us write down the lowest order expansion of  $\delta E$  in terms of a polynomial in the dimensionless couplings  $j_{z\pm}$  and  $j_{\pm\pm}$ . Due to the cubic symmetry of the lattice, the lowest order and most relevant  $U(1)$  symmetry-breaking term is  $\cos(6\phi)^{15,18}$  where  $\phi$  is the azimuthal angle in the  $xy$  plane of the local frame.  $\cos(6\phi) = +1$  and  $-1$  for the  $\psi_2$  and  $\psi_3$  state, respectively, and  $\delta E$  is proportional to the coefficient of  $\cos(6\phi)$ . We note that anisotropy terms of the form  $\sin(6n\phi)$  are absent: using the definition of local  $z$  axis in Fig. 1, an improper four-fold rotation around the global  $z$  axis together with a time reversal transforms  $S_i^x$  to  $S_i^x$  and  $S_i^y$  to  $-S_i^y$ , or  $\phi$  to  $-\phi$ . Since  $\sin(6n\phi)$  is odd under this transformation, such terms are forbidden in the (free) energy.

Since one power of  $S^+$  contributes  $\exp(i\phi)$ , we write down the polynomial expansion of  $\delta E$  with the help of a simple power counting relation,  $j_{\pm\pm} \sim \exp(\pm i2\phi)$  and  $j_{z\pm} \sim$

$\exp(\pm i\phi)$ , getting:

$$\begin{aligned} \delta E &\approx c_3 j_{\pm\pm}^3 + c_2 j_{\pm\pm}^2 j_{z\pm}^2 + c_1 j_{\pm\pm} j_{z\pm}^4 + c_0 j_{z\pm}^6 \\ &\equiv c_3 j_{z\pm}^6 (x^3 + \tilde{c}_2 x^2 + \tilde{c}_1 x + \tilde{c}_0), \end{aligned} \quad (4)$$

where  $x \equiv j_{\pm\pm}/j_{z\pm}^2$ . and the  $c_i$  coefficients are functions of  $j_{zz}$ . Restoring all factors of  $J_{\pm}$ , we have  $x = (J_{\pm} J_{\pm\pm})/J_{z\pm}^2$ . The form (4) is the most general cubic polynomial in  $j_{\pm\pm}$  and  $j_{z\pm}^2$  and the phase boundaries between the  $\psi_2$  and  $\psi_3$  states are determined by the real solutions of Eq. (4) with  $\delta E = 0$ . We therefore expect the number of phase boundaries between  $\psi_2$  and  $\psi_3$  states to evolve smoothly between 1 and 3 as  $j_{zz}$  is varied. We now proceed to explicitly check these expectations on the basis of spin-wave calculations about the  $\psi_2$  and  $\psi_3$  states.

### III. SPIN-WAVE CALCULATIONS

Apprised with the above symmetry-constrained understanding of the phase diagram, we now present the results of our spin-wave calculations. We employ the standard Holstein-Primakoff boson to represent fluctuations about long-range ordered  $\psi_2$  and  $\psi_3$  states. Since the spins point along the local  $x$  and  $y$  direction in  $\psi_2$  or  $\psi_3$ , respectively (see Fig. 1), the spin components in local coordinates are written as:

$$S_i^{(x,y)} = S - a_i^\dagger a_i, \quad (5a)$$

$$S_i^{(y,z)} = \frac{\sqrt{2S}}{2} (a_i^\dagger + a_i), \quad (5b)$$

$$S_i^{(z,x)} = \frac{\sqrt{2S}}{2i} (a_i - a_i^\dagger). \quad (5c)$$

The superscripts  $(\mu, \nu)$  of  $S_i^{(\mu, \nu)}$  correspond to the boson representation for spins in the  $(\psi_2, \psi_3)$  state, respectively. We substitute (5) into (1) and keep terms up to quadratic order in  $a_i$  and  $a_i^\dagger$ . The bosons are written in term of Bloch modes and the spin-wave spectrum is determined in the usual way by a Bogoliubov transformation<sup>25</sup>. We define the total zero-point energy for  $\psi_{2,3}$  states,  $E_0(\psi_{2,3})$  as:

$$E_0(\psi_i) \equiv \frac{1}{N} \sum_{\mathbf{k}} \sum_{\alpha=0}^3 \frac{\hbar \omega_{i\alpha}(\mathbf{k})}{2}, \quad (6)$$

where  $\frac{1}{2} \hbar \omega_{i\alpha}(\mathbf{k})$  is the zero-point energy of the spin-wave mode of momentum  $\mathbf{k}$  for  $\psi_i$  state ( $i = 2, 3$ ).  $\alpha$  labels the spin-wave branches and the summation over  $\mathbf{k}$  is restricted to the first Brillouin zone.  $N$  is the number of primitive tetrahedra units. Some  $\omega_{i\alpha}(\mathbf{k} = 0)$  become imaginary if the interaction parameters puts the system outside the phase boundaries between the  $\Gamma_5$  manifold and the PC or SF long-range ordered states, which both have a  $\mathbf{k} = 0$  ordering wavevector.

We define  $\delta E$  as  $\delta E \equiv E_0(\psi_2) - E_0(\psi_3)$ . Positive or negative  $\delta E$  signals that  $\psi_3$  or  $\psi_2$  is selected by quantum fluctuations, respectively. To check the symmetry arguments in Sec. II, we first calculate  $\delta E(0, j_{\pm\pm})$  and  $\delta E(j_{z\pm}, 0)$  for

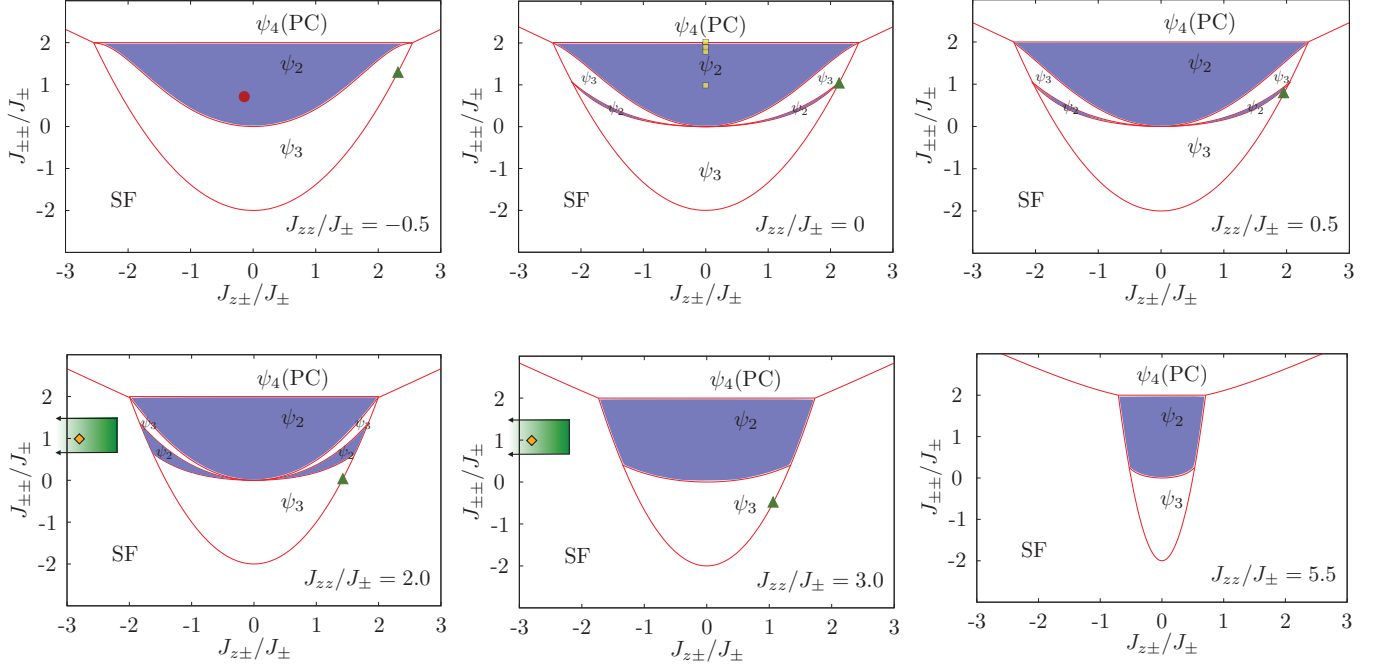


FIG. 3: Phase boundaries separating the  $\psi_2$  and  $\psi_3$  states for different values of  $j_{zz} \equiv J_{zz}/J_{\pm}$ . The solid red lines are phase boundaries between the  $\Gamma_5$  manifold and the Palmer-Chalker (PC, or  $\psi_4$  state of the  $\Gamma_7$  irrep<sup>13</sup>, or the splayed ferromagnetic (SF) state, or, within  $\Gamma_5$ , between the  $\psi_2$  and  $\psi_3$  states. Within the  $\Gamma_5$  manifold,  $\psi_2$  is selected within the blue shaded regions. The various symbols correspond to values of  $J_e \equiv \{J_{\pm}, J_{z\pm}, J_{\pm\pm} \text{ and } J_{zz}\}$  for pyrochlore systems previously studied<sup>12,17,18,21</sup>. The XY antiferromagnet model of Ref.<sup>16</sup> is at  $j_{zz} = j_{z\pm} = 0$  and  $j_{\pm\pm} = 2$ , that is at the  $\psi_2$  (PC) boundary where quantum fluctuations select  $\psi_2$ <sup>16,17</sup>. The red circle in  $\psi_2$  ( $J_{zz}/J_{\pm} = -0.5$  panel) is for  $\text{Er}_2\text{Ti}_2\text{O}_7$ <sup>18</sup>. Despite uncertainties in its  $J_e$  couplings, we find that  $\text{Er}_2\text{Ti}_2\text{O}_7$  remains deeply in the  $\psi_2$  region and does not cross in either  $\psi_3$  or  $\psi_4$  (PC). The yellow squares in  $\psi_2$  ( $J_{zz}/J_{\pm} = 0$  panel) are for the model of Ref. [17] with anisotropic coupling  $j_a \equiv J_a/J$  in their notation. With  $J_{\pm\pm}/J_{\pm} = (4 - j_a)/(2 + j_a)$ , their model approaches the  $\psi_2$  (PC) boundary as  $j_a \rightarrow 0^+$ . The green triangle ( $J_{zz}/J_{\pm} = -0.5$ ,  $J_{zz}/J_{\pm} = 0$ ,  $J_{zz}/J_{\pm} = 0.5$ ,  $J_{zz}/J_{\pm} = 2.0$ ,  $J_{zz}/J_{\pm} = 3.0$  panels) on the  $\psi_3$ /SF boundary is for the Heisenberg pyrochlore antiferromagnet with indirect Dzyaloshinskii-Moriya interactions<sup>15</sup> of varying strength studied in Ref. [21] which, coincidentally, resides on the  $\Gamma_5$ /SF boundary at the classical level (Appendix A). The orange diamond corresponds to  $\text{Yb}_2\text{Ti}_2\text{O}_7$ <sup>12</sup>. Because of the uncertainty in  $J_{\pm}, J_{z\pm}, J_{\pm\pm}$  and  $J_{zz}$ ,  $\text{Yb}_2\text{Ti}_2\text{O}_7$  “inhabits” the  $J_{zz}/J_{\pm} = 2.0$  and  $J_{zz}/J_{\pm} = 3.0$  panels. The green box delineates the ranges  $J_{\pm\pm}/J_{\pm} \in [0.6, 1.5]$  and  $J_{z\pm}/J_{\pm} \in [-3.8, -2.2]$ , which extends well to the left of the vertical  $J_{\pm\pm}/J_{\pm}$  axis, hence the left pointing arrows. This figure illustrates that the Hamiltonian of  $\text{Yb}_2\text{Ti}_2\text{O}_7$  sits in the same SF phase recently reported for  $\text{Yb}_2\text{Sn}_2\text{O}_7$ <sup>24</sup>, far from the  $\Gamma_5$  manifold ( $\psi_2$  and  $\psi_3$ ) as well as the  $\psi_4$  (PC) state.

$j_{zz} = 0$ . As shown in Fig. 2,  $\delta E(0, j_{\pm\pm}) \sim j_{\pm\pm}^3$  and  $\delta E(J_{z\pm}, 0) \sim j_{z\pm}^6$ , consistent with Eq. (4).

We then scan the  $j_{z\pm}$  and  $j_{\pm\pm}$  parameter space for several values of  $j_{zz}$ . The results are shown in Fig. 3, which constitutes our main result. There is only one phase boundary dividing regions of  $\psi_2$  and  $\psi_3$  states for large negative and positive  $j_{zz}$ . For intermediate values of  $j_{zz}$ ,  $0 \lesssim j_{zz} \lesssim 3$  we observe *three phase boundaries* separating alternating regions of  $\psi_2$  and  $\psi_3$ . As  $j_{zz} \rightarrow 3$  from below, the (lower) narrow  $\psi_2$  sliver region, sandwiched between two  $\psi_3$  regions, expands and merges with the large  $\psi_2$  region for  $j_{zz} \sim 3$ . Also, the same narrow  $\psi_2$  sliver disappears rapidly for  $j_{zz} \lesssim 0$ . As expected, all phase boundaries touch at  $j_{z\pm} = j_{\pm\pm} = 0$  for arbitrary  $j_{zz}$ . No other phases but  $\psi_2$  and  $\psi_3$  were found stabilized by quantum fluctuations within the  $\Gamma_5$  manifold.

It is appropriate at this point to comment on the role of higher order anisotropic terms in  $\delta E(\phi)$ . While we expect higher order corrections to  $\delta E$  beyond  $\cos(6\phi)$  of the form  $\sum_{n>0} g_{2n+1} \cos\{6(2n+1)\phi\}$  (terms such as  $\cos(12n\phi)$  do

not distinguish  $\psi_2$  and  $\psi_3$ ), these do not lead to qualitative new behavior for the  $J_{\pm\pm}/J_{\pm}$  vs  $J_{z\pm}/J_{\pm}$  phase diagram on the basis of our spin-wave calculations. In particular, *no more* than three  $\psi_2/\psi_3$  phase boundaries are observed in our explicit quantum spin wave calculations, in agreement with the heuristic arguments leading to Eq.(4). One does note in the insets of Fig. 2 deviations of  $\delta E$ , for either large  $J_{z\pm}/J_{\pm}$  or  $J_{\pm\pm}/J_{\pm}$ , away from the strict power laws ( $\sim J_{z\pm}^6$  and  $\sim J_{\pm\pm}^3$ ) behaviors expected on the basis of the lowest  $\cos(6\phi)$  harmonic (i.e. Eq. (4)). Referring to Fig. 3, the roots of the Eq. (4),  $\delta E = 0$ , would give for the  $\psi_2/\psi_3$  phase boundaries  $j_{\pm\pm} = \omega_{\mu}(J_{zz})j_{z\pm}^2$  (where  $\mu = 1, 2, 3$  and  $\omega_{\mu}$  a real number). This form would lead to a gap between the boundaries defining the narrow  $\psi_2$  sliver that would *monotonously* widen as  $j_{z\pm}$  increases if the cubic Eq. (4) for  $\delta E$  was exact. However, as can be seen in Fig. 3 for  $J_{zz}/J_{\pm} = -0.5$  and  $J_{zz}/J_{\pm} = 0$ , the width of the sliver first grows as  $J_{z\pm}/J_{\pm}$  increases, reaches a maximum width, and then *narrows* as the classical boundary  $\Gamma_5$ /SF boundary given by Eq. (2) is ap-



proached from inside the  $\Gamma_5$  region. It therefore appears that the corrections to  $\delta E$  beyond  $\cos(6\phi)$  merely lead to a slight renormalization of the “internal” (i.e. within the  $\Gamma_5$  region)  $\psi_2/\psi_3$  phase boundaries defining the narrow  $\psi_2$  sliver in the  $J_{zz}/J_{\pm} = 0, 0.5$  and  $2.0$  panels of Fig. 3.

#### IV. THE ROLE OF LONG-RANGE DIPOLAR INTERACTION IN $\text{Er}_2\text{Ti}_2\text{O}_7$

Our knowledge of the general phase diagram in Fig 3 for anisotropic nearest-neighbor exchange  $J_e = \{J_{\pm}, J_{\pm\pm}, J_{z\pm}, J_{zz}\}$  motivates us to return to an important material-relevant question: what is the role of the long-range  $1/r^3$  magnetostatic dipole-dipole interaction in allowing for a  $\psi_2$  ground state induced by quantum ObD in  $\text{Er}_2\text{Ti}_2\text{O}_7$ ?<sup>7,11,13</sup> The magnetic moment of  $\text{Er}^{3+}$  in the local  $XY$  plane is approximately  $3 \mu_B$ .<sup>7</sup> As a result, the strength of the nearest-neighbor part of the dipolar interaction is of the order of 15% to 50% of the  $J_e$  parameters determined in Ref.[18]. It is therefore natural to ask whether the dipolar interaction beyond the nearest-neighbor affects the quantum ObD, proposed to be at play in  $\text{Er}_2\text{Ti}_2\text{O}_7$ .<sup>17,18</sup>

To address this question, we adopt the values of  $J_e = \{J_{zz}, J_{\pm}, J_{\pm\pm}, J_{z\pm}\}$  with their uncertainty from Savary *et al.*<sup>18</sup>. In order to avoid a double accounting of the nearest-neighbor contribution from the dipoles implicitly contained in the experimentally determined  $J_e$ , we need to subtract the nearest-neighbor contribution from the dipolar interaction from the  $J_e$  determined in Ref. [18].

Working with bare couplings, the nearest-neighbor part of the dipolar Hamiltonian is:

$$\mathcal{H}^{\text{dip}} = D \sum_{\langle ab \rangle} \left[ \frac{\mathbf{S}_a \cdot \mathbf{S}_b}{|\mathbf{R}_{ab}|^3} - 3 \frac{(\mathbf{S}_a \cdot \mathbf{R}_{ab})(\mathbf{S}_b \cdot \mathbf{R}_{ab})}{|\mathbf{R}_{ab}|^5} \right] \quad (7)$$

where

$$D = \frac{\mu_0 \mu_B^2}{4\pi}. \quad (8)$$

Here  $\mu_0$  is the permeability of free space,  $\mu_B$  is the Bohr magneton, and  $a_0 = 10.07 \text{ \AA}$ <sup>8,26</sup> is the conventional cubic unit cell lattice constant of  $\text{Er}_2\text{Ti}_2\text{O}_7$ . The nearest-neighbor distance  $|\mathbf{R}_{ab}| = a_0\sqrt{2}/4$ .

Translating the dipolar interaction into a  $\{J_{zz}^{\text{dip}}, J_{\pm}^{\text{dip}}, J_{\pm\pm}^{\text{dip}}, J_{z\pm}^{\text{dip}}\}$  notation, we obtain the following couplings for the dipolar contribution to the nearest-neighbor interactions:

$$\begin{pmatrix} J_{zz}^{\text{dip}} \\ J_{\pm}^{\text{dip}} \\ J_{\pm\pm}^{\text{dip}} \\ J_{z\pm}^{\text{dip}} \end{pmatrix} = \frac{D}{12} \begin{pmatrix} 20g_z^2 \\ -g_{xy}^2 \\ 7g_{xy}^2 \\ -2\sqrt{2}g_{xy}g_z \end{pmatrix} \quad (9)$$

where  $g_{xy}$  and  $g_z$  are the perpendicular and longitudinal  $g$ -tensors with respect to the local  $[111]$  direction, respectively. We subtract these dipolar contributions from the experimental  $\{J_{zz}, J_{\pm}, J_{\pm\pm}, J_{z\pm}\}$  couplings in Savary *et al.*<sup>18</sup>.

The nearest-neighbor dipole couplings we find for the best-fit couplings and  $g$ -tensors reported in Ref. [18] are ( $g$ -tensored values in  $10^{-2}$  meV)

$$\begin{pmatrix} J_{zz}^{\text{dip}} \\ J_{\pm}^{\text{dip}} \\ J_{\pm\pm}^{\text{dip}} \\ J_{z\pm}^{\text{dip}} \end{pmatrix} = \begin{pmatrix} 1.18997 \\ -0.353283 \\ 2.47298 \\ -0.410071 \end{pmatrix}. \quad (10)$$

These values differ slightly from the values  $(0.8, -0.46, 3.2, -0.38)$  reported in the Supplementary material of Ref. [18] as the authors of that paper did not use their own best fitted  $g$ -tensor values for their calculation of the  $J_{uv}^{\text{dip}}$  values.

We next proceed to calculate the spin-wave spectrum including long-range dipolar interaction following the method of Ref. [25] using either  $\psi_2$  or  $\psi_3$  as reference (degenerate) classical ground state. The Fourier transformation of the long-range dipolar interaction is evaluated using Ewald summation<sup>25,27</sup>. The calculation is carried out for a total of  $3^6 = 729$  sets of couplings and  $g$ -tensor values within the following ranges reported in Ref. [18]:  $J_{zz} = -2.5 \pm 1.8$ ,  $J_{\pm} = 6.5 \pm 0.75$ ,  $J_{\pm\pm} = 4.2 \pm 0.5$ ,  $g_{xy} = 5.97 \pm 0.08$ , and  $g_z = 2.45 \pm 0.23$ . For *all* 729 combinations of these six quantities, our calculations show that the ground state of  $\text{Er}_2\text{Ti}_2\text{O}_7$  is  $\psi_2$  when the long-range dipolar interactions are properly accounted for.

While the  $J_{uv}^{\text{dip}}$  couplings in Eq. (10) are not small compared to the experimental  $J_{uv}^e$  determined in Ref. [18], the conclusion that quantum order-by-disorder into  $\psi_2$  is operational for  $\text{Er}_2\text{Ti}_2\text{O}_7$  is unchanged because the material “resides” deeply in the  $\psi_2$  state of the phase diagram of Fig. 3 ( $J_{zz}/J_{\pm} = -0.5$  panel). That being said, we would expect that consideration of the long-range dipolar interaction would renormalize the spin-wave gap – a necessary signature of the broken discrete symmetry  $\psi_2$  state<sup>16</sup> – computed in Ref. [18].

The conclusion of Ref. [18] that quantum ObD is responsible for the  $\psi_2$  ground state for the nearest-neighbor  $J_e$  exchange parameters determined by inelastic neutron scattering is thus upheld. This is the main result of our work as per the ground state of  $\text{Er}_2\text{Ti}_2\text{O}_7$ .

#### V. DISCUSSION

In this work, we studied the quantum order-by-disorder for a pyrochlore  $XY$  magnet with  $J_e = \{J_{\pm}, J_{z\pm}, J_{\pm\pm}, J_{zz}\}$  exchange couplings between effective spin-1/2 degrees of freedom. We determined the region of  $J_e$  interaction parameters where the classically degenerate  $\Gamma_5$  manifold is the ground state by minimizing the classical energy. Within the  $\Gamma_5$  manifold, the boundaries between the  $\psi_2$  and  $\psi_3$  states are obtained by comparing the contribution of zero-point energy from spin waves to the total energy of the system. We recover the results of several previous works<sup>16–18,21</sup> as special cases of our study (see caption of Fig. 3).

We exposed that there can be one or three phase boundaries depending on the value of  $J_{zz}$ . This observation was

anticipated since the number of  $\psi_2/\psi_3$  phase boundaries is accurately controlled by the number of real solutions of the cubic Eq. (4). While the exact location of the phase boundaries are expected to shift if interactions between spin-waves are included or the temperature is finite, the topology of the phase diagram is, however, governed by the symmetry arguments presented in this paper. Guided by these arguments, it would be interesting to explore how the phase boundaries between  $\psi_2$  and  $\psi_3$  states evolve with temperature. Such a phenomenon was studied in Ref. [21] where  $\psi_2$  order below and near the critical temperature changes to  $\psi_3$  order at lower temperature. We expect such a scenario to occur in materials close to one of the  $\psi_2/\psi_3$  zero temperature phase boundaries. In addition, we speculate that  $\text{Er}_2\text{Sn}_2\text{O}_7$  may be close to one of the  $\psi_2/\psi_3$  phase boundaries, where the selection of either state can become weak, or close to the  $\psi_2/\text{PC}$  boundary near  $J_{\pm\pm}/J_{\pm} = 2$ . This could help explain why  $\text{Er}_2\text{Sn}_2\text{O}_7$  fails to order down to 50 mK<sup>28–30</sup>.

Other possibilities for exploring the physics of  $XY$  pyrochlore magnets may include  $\text{Er}_2\text{Ge}_2\text{O}_7$  and  $\text{Yb}_2\text{Ge}_2\text{O}_7$ <sup>31</sup>. It may also be possible that some of the aforementioned phases may be realized in materials other than the  $R_2\text{M}_2\text{O}_7$  pyrochlore oxides<sup>6</sup>. For example, the  $\text{CdR}_2\text{Se}_2$  and  $\text{CdR}_2\text{S}_2$  chalcogenide spinel compounds, in which the  $R$  trivalent rare-earth ions sit on a regular pyrochlore lattice of corner-sharing tetrahedra, provide a new opportunity for the study of frustrated magnetism on the pyrochlore lattice<sup>32</sup>. By rescaling the crystal field parameters determined for the spinel-based spin ice compound  $\text{CdEr}_2\text{Se}_4$ <sup>33</sup>, we predict (Appendix B) that the  $\text{Dy}^{3+}$  ions in the sister compound  $\text{CdDy}_2\text{Se}_4$  would be  $XY$ -like and could possibly realize some of the interesting physics described above.

Given the rich phase diagram of Fig. 3, especially that of the  $\Gamma_5$  manifold, it would be interesting to investigate whether transitions between  $\psi_2$  and  $\psi_3$  states can be driven by various control parameters. This includes external magnetic field along different symmetry directions<sup>9</sup>, hydrostatic<sup>34,35</sup> or chemical pressure<sup>36</sup> as well as random disorder, being either “intrinsic” and caused by magnetic rare-earth ions substituting for the transition metal ion (e.g.  $\text{Ti}^{4+}$ , dubbed as “stuffing”)<sup>37</sup> or “extrinsic” and driven by diluting the  $\text{Er}^{3+}$  sites by non-magnetic  $\text{Y}^{3+}$  ions, for example<sup>38,39</sup>. With the deeper understanding of quantum ObD in  $XY$  pyrochlore magnets reached in the present work, we hope that our work will stimulate further systematic experimental and theoretical studies of  $XY$  pyrochlore oxides and spinel materials.

## ACKNOWLEDGEMENT

M.G. acknowledges Ludovic Jaubert for a stimulating discussion regarding the problem of degeneracy and order-by-disorder in  $XY$  pyrochlore magnets. We thank Alexandre Day, Behnam Javanparast, Jaan Oitmaa and Rajiv Singh for useful discussions and related collaborations and acknowledge Boris Malkin for useful correspondence. We thank Tao-ran Lin for help with the figures. This work was supported by the NSERC of Canada, the Canada Research Chair program

(M.G., Tier 1), and the Perimeter Institute (PI) for Theoretical Physics. Research at PI is supported by the Government of Canada through Industry Canada and by the Province of Ontario through the Ministry of Economic Development & Innovation.

## Appendix A: TRANSLATION BETWEEN DIFFERENT CONVENTIONS

The Hamiltonians of Ref. [17] and [21] are, respectively:

$$\mathcal{H}_Z = \sum_{\langle ij \rangle} \left[ \left( \mathcal{J} + \frac{\mathcal{J}_a}{3} \right) \mathbf{S}_i^\perp \cdot \mathbf{S}_j^\perp - \frac{\mathcal{J}_a}{3} (\mathbf{S}_i^\perp \cdot \mathbf{S}_j^\perp - 3 (\mathbf{S}_i^\perp \cdot \hat{\mathbf{r}}_{ij}) (\mathbf{S}_j^\perp \cdot \hat{\mathbf{r}}_{ij})) \right], \quad (\text{A1a})$$

$$\mathcal{H}_C = \sum_{\langle ij \rangle} \left[ J (\mathbf{S}_i \cdot \mathbf{S}_j) + D \left( \hat{\mathbf{n}}_{ij}^{\text{DM}} \cdot \mathbf{S}_i \times \mathbf{S}_j \right) \right]. \quad (\text{A1b})$$

Here the superscript  $\perp$  denotes the component perpendicular to the local [111] axes (i.e. the  $XY$  model).  $\hat{\mathbf{r}}_{ij}$  is the unit vector pointing from site  $i$  to site  $j$ .  $D$  is the strength of Dzyaloshinskii-Moriya (DM) interaction.  $\hat{\mathbf{n}}_{ij}^{\text{DM}}$  is the DM vector<sup>40</sup> on bond  $\langle ij \rangle$  such that  $D > 0$  corresponds to *indirect* DM interaction. We first translate  $\mathcal{J}$  and  $\mathcal{J}_a$  in  $\mathcal{H}_Z$  of Ref. [17] above:

$$J_{\pm} = \frac{\mathcal{J}}{6} + \frac{\mathcal{J}_a}{12}, \quad J_{\pm\pm} = \frac{\mathcal{J}}{3} - \frac{\mathcal{J}_a}{12}, \quad J_{zz} = J_{z\pm} = 0. \quad (\text{A2})$$

As a result,  $j_{\pm\pm} = (4\mathcal{J} - \mathcal{J}_a)/(2\mathcal{J} + \mathcal{J}_a)$  and  $j_{zz} = j_{z\pm} = 0$ .

We note here that had Ref. [17] considered  $\mathcal{J}_a > 4$ , we predict from the results in Fig. 3 that they would have observed order-by-disorder in  $\psi_3$ .

We now translate  $J$  and  $D$  in the Hamiltonian  $\mathcal{H}_C$  of Ref. [21] above:

$$J_{\pm} = \frac{J}{6} + \frac{\sqrt{2}D}{6}, \quad J_{\pm\pm} = \frac{J}{3} - \frac{\sqrt{2}D}{6}, \quad (\text{A3})$$

$$J_{zz} = -\frac{J}{3} + \frac{2\sqrt{2}D}{3}, \quad J_{z\pm} = \frac{\sqrt{2}J}{3} + \frac{D}{6}.$$

Consequently, we have:

$$j_{\pm\pm} = \frac{2J - \sqrt{2}D}{J + \sqrt{2}D}, \quad (\text{A4a})$$

$$j_{zz} = \frac{-2J + 4\sqrt{2}D}{J + \sqrt{2}D}, \quad (\text{A4b})$$

$$j_{z\pm} = \frac{2\sqrt{2}J + D}{J + \sqrt{2}D}. \quad (\text{A4c})$$

For  $0 < D < \infty$ ,  $-2 < j_{zz} < 4$ .

Below we define  $\gamma_{ij}$  and  $\zeta_{ij}$  in the convention of Ref. [12]. The pyrochlore lattice has four sublattices 0, 1, 2 and 3. Both  $\gamma_{ij}$  and  $\zeta_{ij}$  are labeled by the sublattices site  $i$  and  $j$  belong

to.

$$\gamma_{01} = -\zeta_{01}^* = \gamma_{23} = -\zeta_{23}^* = 1, \quad (\text{A5a})$$

$$\gamma_{02} = -\zeta_{02}^* = \gamma_{13} = -\zeta_{13}^* = \exp\left(\frac{2\pi i}{3}\right), \quad (\text{A5b})$$

$$\gamma_{03} = -\zeta_{03}^* = \gamma_{12} = -\zeta_{12}^* = \exp\left(-\frac{2\pi i}{3}\right). \quad (\text{A5c})$$

## Appendix B: EXPECTED EFFECTIVE XY SPIN FOR $\text{Dy}^{3+}$ in $\text{CdDy}_2\text{Se}_4$ SPINEL

Recent work<sup>33</sup> has shown that in  $\text{CdEr}_2\text{Se}_2$ , the  $\text{Er}^{3+}$  can be described by a classical Ising spin (with  $g_{zz} = 16.05$ , and  $g_{xy} = 0$ ), with the system displaying a residual Pauling entropy and is thus a spin ice compound<sup>1,6</sup>. The effective pseudospin-1/2 anisotropy, or components of the  $g$ -tensors, of a ground-state doublet are determined from the crystal field Hamiltonian,  $\mathcal{H}_{\text{cf}}$ , acting on the rare-earth ion. Ref. [33] provides an estimate of the parameters that determine  $\mathcal{H}_{\text{cf}}$  for  $\text{CdEr}_2\text{Se}_2$ . This, in return, allows one to roughly estimate the crystal field parameters of other rare-earth ions in a same isostructural family. Here, we are particularly interested in  $\text{CdDy}_2\text{Se}_4$  studied in Ref. [32].

The crystal field Hamiltonian,  $\mathcal{H}_{\text{cf}}$  acting on a rare-earth can be written as

$$\mathcal{H}_{\text{cf}} = \sum_i \sum_{l,m} \tilde{B}_l^m O_l^m(\mathbf{J}_i), \quad (\text{B1})$$

where the  $\tilde{B}_l^m$  are the crystal field parameters and the  $O_l^m(\mathbf{J}_i^z, \mathbf{J}_i^\pm)$  are the Stevens equivalent operators functions of the components  $J_i^z$  and  $J_i^\pm$  of the angular momentum<sup>41,42</sup>.

In the so-called Stevens formalism,  $\tilde{B}_2^0 \approx \alpha_J \langle r^2 \rangle A_2^0$ , where  $A_2^0$  is a point charge lattice sum representing the crystal-field,

$\langle r^2 \rangle$  the expectation value of  $r^2$  for the 4f electrons, and where we neglected the so-called charge shielding factor<sup>6</sup>. As discussed in Ref. [6], the  $\alpha_J$  Stevens factor<sup>41,42</sup> changes sign in a systematic pattern throughout the lanthanide series. It is positive for Sm, Er, Tm and Yb and negative for all others. So, the sign of  $\tilde{B}_2^0$  depends on the product  $\alpha_J A_2^0$ . As Ref. [33] finds  $A_2^0 < 0$ <sup>43</sup> for  $\text{Er}^{3+}$  in  $\text{CdEr}_2\text{Se}_4$ , a key factor for making  $\text{Er}^{3+}$  Ising-like in this compound, we thus expect  $\tilde{B}_2^0$  to be positive for  $\text{Dy}^{3+}$  in  $\text{CdDy}_2\text{Se}_4$ <sup>32</sup>, thus suggesting that  $\text{Dy}^{3+}$  would be XY-like in  $\text{CdDy}_2\text{Se}_4$ .

To investigate this suggestion further, we take the  $A_l^m$  coefficients ( $B_l^m$  in the notation of Ref. [33,43]) and, using the Stevens factors for  $\text{Er}^{3+}$  and  $\text{Dy}^{3+}$ <sup>42</sup>, the  $\langle r^n \rangle$  radial expectation values for  $\text{Er}^{3+}$  and  $\text{Dy}^{3+}$  taken from Ref. [44], we can estimate the  $\tilde{B}_l^m$  in Eq. (B1) for  $\text{CdDy}_2\text{Se}_4$ . We find  $\tilde{B}_2^0 = -260.95$ ,  $\tilde{B}_4^0 = -957.65$ ,  $\tilde{B}_4^3 = -1139.5$ ,  $\tilde{B}_6^0 = 167.93$ ,  $\tilde{B}_6^3 = -256.97$  and  $\tilde{B}_6^6 = 142.96$ , all in K units. We then proceed to diagonalize  $\mathcal{H}_{\text{cf}}$ , finding a ground state doublet with  $g$ -tensor components  $g_{zz} = 3.36$  and  $g_{xy} = 8.19$ , with an energy gap of  $\Delta = 18.1$  K from the lowest energy excited doublet.

With  $g_{xy}/g_{zz} \sim 2.4$ , we are thus led to anticipate that the  $\text{CdDy}_2\text{Se}_4$ <sup>32</sup> might constitute an interesting realization of magnetic system described by a pseudospin-1/2 Hamiltonian such as Eq. (1) in the main text, and whose thermodynamic properties may be rationalized on the basis of the discussion presented in the paper. In particular, being an XY system, it may display a phenomenon of quantum order-by-disorder if its exchange parameters  $J_e$  position it in the  $\Gamma_5$  phase diagram of Fig. (3) in the main text. Alternatively, depending on its  $J_e$  couplings, it may find itself in either a  $\psi_4$  or SF phase or even allow for a more exotic possibility, and display a  $U(1)$  quantum spin liquid or Coulomb ferromagnet as discussed in Ref. [20].

<sup>1</sup> C. Lacroix, P. Mendels, and F. Mila, eds., *Introduction to Frustrated Magnetism* (Springer, 2011).

<sup>2</sup> J. Villain, R. Bidaux, J.-P. Carton, and R. Conte, J. Phys. France **41**, 1263 (1980).

<sup>3</sup> E. F. Shender, Sov. Phys. JETP **56** (1982).

<sup>4</sup> C. L. Henley, Phys. Rev. Lett. **62**, 2056 (1989).

<sup>5</sup> T. Yildirim, Turkish Journal of Physics **23**, 47 (1999).

<sup>6</sup> J. S. Gardner, M. J. P. Gingras, and J. E. Greedan, Rev. Mod. Phys. **82**, 53 (2010).

<sup>7</sup> J. D. M. Champion, M. J. Harris, P. C. W. Holdsworth, A. S. Wills, G. Balakrishnan, S. T. Bramwell, E. Čížmár, T. Fennell, J. S. Gardner, J. Lago, et al., Phys. Rev. B **68**, 020401 (2003).

<sup>8</sup> H. W. J. Blöte, R. Wielinga, and W. J. Huiskamp, Physica **43**, 549 (1969).

<sup>9</sup> J. P. C. Ruff, J. P. Clancy, A. Bourque, M. A. White, M. Ramazanoglu, J. S. Gardner, Y. Qiu, J. R. D. Copley, M. B. Johnson, H. A. Dabkowska, et al., Phys. Rev. Lett. **101**, 147205 (2008).

<sup>10</sup> S. S. Sosin, L. A. Prozorova, M. R. Lees, G. Balakrishnan, and O. A. Petrenko, Phys. Rev. B **82**, 094428 (2010).

<sup>11</sup> P. Dalmas de Réotier, A. Yaouanc, Y. Chapuis, S. H. Curnoe,

B. Grenier, E. Ressouche, C. Marin, J. Lago, C. Baines, and S. R. Giblin, Phys. Rev. B **86**, 104424 (2012).

<sup>12</sup> K. A. Ross, L. Savary, B. D. Gaulin, and L. Balents, Phys. Rev. X **1**, 021002 (2011).

<sup>13</sup> A. Poole, A. S. Wills, and E. Lelièvre-Berna, Journal of Physics: Condensed Matter **19**, 452201 (2007).

<sup>14</sup> J. D. M. Champion and P. C. W. Holdsworth, Journal of Physics: Condensed Matter **16**, S665 (2004).

<sup>15</sup> P. A. McClarty, S. H. Curnoe, and M. J. P. Gingras, Journal of Physics: Conference Series **145**, 012032 (2009).

<sup>16</sup> P. Stasiak, P. A. McClarty, and M. J. P. Gingras, ArXiv e-prints (2011), 1108.6053.

<sup>17</sup> M. E. Zhitomirsky, M. V. Gvozdkova, P. C. W. Holdsworth, and R. Moessner, Phys. Rev. Lett. **109**, 077204 (2012).

<sup>18</sup> L. Savary, K. A. Ross, B. D. Gaulin, J. P. C. Ruff, and L. Balents, Phys. Rev. Lett. **109**, 167201 (2012).

<sup>19</sup> See, however, Ref. [15] for a discussion of a weak energetic mechanism operating at the mean-field level and proceeding via the excited crystal field states.

<sup>20</sup> L. Savary and L. Balents, Phys. Rev. Lett. **108**, 037202 (2012).

- <sup>21</sup> G.-W. Chern, ArXiv e-prints (2010), 1008.3038.
- <sup>22</sup> S. T. Bramwell and M. J. Harris, *Journal of Physics: Condensed Matter* **10**, L215 (1998).
- <sup>23</sup> S. E. Palmer and J. T. Chalker, *Phys. Rev. B* **62**, 488 (2000).
- <sup>24</sup> A. Yaouanc, P. Dalmas de Réotier, P. Bonville, J. A. Hodges, V. Glazkov, L. Keller, V. Sikolenko, M. Bartkowiak, A. Amato, C. Baines, et al., *Phys. Rev. Lett.* **110**, 127207 (2013).
- <sup>25</sup> A. G. D. Maestro and M. J. P. Gingras, *Journal of Physics: Condensed Matter* **16**, 3339 (2004).
- <sup>26</sup> O. Knop, F. Brisse, and L. Castelliz, *Canadian Journal of Chemistry* **43**, 2812 (1965).
- <sup>27</sup> M. Enjalran and M. J. P. Gingras, *Phys. Rev. B* **70**, 174426 (2004).
- <sup>28</sup> J. Lago, T. Lancaster, S. J. Blundell, S. T. Bramwell, F. L. Pratt, M. Shirai, and C. Baines, *Journal of Physics: Condensed Matter* **17**, 979 (2005).
- <sup>29</sup> P. M. Sarte, H. J. Silverstein, B. T. K. V. Wyk, J. S. Gardner, Y. Qiu, H. D. Zhou, and C. R. Wiebe, *Journal of Physics: Condensed Matter* **23**, 382201 (2011).
- <sup>30</sup> S. Guitteny, S. Petit, E. Lhotel, J. Robert, P. Bonville, A. Forget, and I. Mirebeau, ArXiv e-prints (2013), 1307.1636.
- <sup>31</sup> A. Hallas, H. D. Zhou, A. A. Lopez, H. J. Silverstein, J. P. Attfield, and C. R. Wiebe, <http://meetings.aps.org/Meeting/MAR13/Session/T15.13> (2013).
- <sup>32</sup> G. C. Lau, R. S. Freitas, B. G. Ueland, P. Schiffer, and R. J. Cava, *Phys. Rev. B* **72**, 054411 (2005).
- <sup>33</sup> J. Lago, I. Živković, B. Z. Malkin, J. Rodriguez Fernandez, P. Ghigna, P. Dalmas de Réotier, A. Yaouanc, and T. Rojo, *Phys. Rev. Lett.* **104**, 247203 (2010).
- <sup>34</sup> I. Mirebeau, I. N. Goncharenko, P. Cadavez-Peres, S. T. Bramwell, M. J. P. Gingras, and J. S. Gardner, *Nature* **420**, 547 (2002).
- <sup>35</sup> I. Mirebeau, I. Goncharenko, H. Cao, and A. Forget, *Phys. Rev. B* **80**, 220407 (2009).
- <sup>36</sup> H. D. Zhou, J. G. Cheng, A. M. Hallas, C. R. Wiebe, G. Li, L. Balicas, J. S. Zhou, J. B. Goodenough, J. S. Gardner, and E. S. Choi, *Phys. Rev. Lett.* **108**, 207206 (2012).
- <sup>37</sup> K. A. Ross, T. Proffen, H. A. Dabkowska, J. A. Quilliam, L. R. Yaraskavitch, J. B. Kycia, and B. D. Gaulin, *Phys. Rev. B* **86**, 174424 (2012).
- <sup>38</sup> X. Ke, R. S. Freitas, B. G. Ueland, G. C. Lau, M. L. Dahlberg, R. J. Cava, R. Moessner, and P. Schiffer, *Phys. Rev. Lett.* **99**, 137203 (2007).
- <sup>39</sup> T. Lin, X. Ke, M. Thesberg, P. Schiffer, R. G. Melko, and M. J. P. Gingras, ArXiv e-prints (2013), 1303.7240.
- <sup>40</sup> M. Elhajal, B. Canals, R. Sunyer, and C. Lacroix, *Phys. Rev. B* **71**, 094420 (2005).
- <sup>41</sup> K. Stevens, *Proceedings of the Physical Society. Section A* **65**, 209 (1952).
- <sup>42</sup> M. Hutchings (Academic Press, 1964), vol. 16 of *Solid State Physics*, pp. 227 – 273.
- <sup>43</sup> The literature of crystal field physics and Hamiltonian is plagued with confusing notation. For example, Ref. [33] uses crystal field parameters  $B_{lm}$  for the tensorial operators  $C_l^m$ . To avoid confusion, we refer to these as  $A_l^m$  above. The transformations from the crystal field parameters  $A_l^m$  (or  $B_l^m$  in Ref. [33]) and the  $\tilde{B}_l^m$  in the Stevens formalism employed above are given in A. J. Kassman, *J. Chem. Phys.* **53**, 4118 (1970).
- <sup>44</sup> A. Freeman and J. Desclaux, *Journal of Magnetism and Magnetic Materials* **12**, 11 (1979).